Colloids and Surfaces B: Biointerfaces 215 (2022) 112493

Contents lists available at ScienceDirect

Colloids and Surfaces B: Biointerfaces

journal homepage: www.elsevier.com/locate/colsurfb

Partially fluorinated nanoemulsions for ^{19}F MRI-fluorescence dual imaging cell tracking

Kexin Chen [a,b,1], Tingjuan Wu [a,b,1], Mou Jiang [c], Anfeng Li [a,b], Xingxing Peng [a,b], Shizhen Chen [c], Zhigang Yang [b], Xin Zhou [c], Xing Zheng [a,*], Zhong-Xing Jiang [b,c,**]

[a] Group of Lead Compound, Department of Pharmacy, Hunan Provincial Key Laboratory of Tumor Microenvironment Responsive Drug Research, Hunan Province Cooperative Innovation Center for Molecular Target New Drug Study, University of South China, Hengyang 421001, China

[b] Hubei Province Engineering and Technology Research Center for Fluorinated Pharmaceuticals, School of Pharmaceutical Sciences, Wuhan University, Wuhan 430071, China

[c] State Key Laboratory of Magnetic Resonance and Atomic and Molecular Physics, National Center for Magnetic Resonance in Wuhan, Wuhan Institute of Physics and Mathematics, Innovation Academy for Precision Measurement Science and Technology, Chinese Academy of Sciences-Wuhan National Laboratory for Optoelectronics, Huazhong University of Science and Technology, Wuhan 430071, China

ARTICLE INFO

Keywords:
^{19}F magnetic resonance imaging
Fluorescence imaging
Nanoemulsions
Paramagnetic effect
Cell tracking

ABSTRACT

Fluorine-19 magnetic resonance imaging (^{19}F MRI) has been a technology of choice for in vivo cell tracking, in which perfluorocarbons (PFCs) nanoemulsions are the most used ^{19}F MRI agents. However, the peculiar physicochemical properties of PFCs may lead to poor cell uptake and misleading cell tracking results. Herein, we employed partially fluorinated aromatic agents to formulate paramagnetic nanoemulsions as novel ^{19}F MRI-fluorescence (FL) dual imaging agents for cell tracking. With the intramolecular π-π interaction, low density and fluorine content, the partially fluorinated agents enable considerable solubilities of functional agents and short relaxation times, which facilitates convenient preparation of stable, biocompatible, and multifunctional nanoemulsions with high ^{19}F MRI sensitivity. Replacing PFCs in ^{19}F MRI nanoemulsions with readily available partially fluorinated aromatic agents may address many issues associated with PFCs and provide a novel strategy for high-performance ^{19}F MRI agents of broad biomedical applications.

1. Introduction

In recent years, ^{19}F magnetic resonance imaging (^{19}F MRI) has been increasingly used in biomedicine. As a highly selective and quantitative imaging technology, ^{19}F MRI provides in vivo images without background interference, ionizing radiation, and tissue depth limit [1–3], which are advantageous over many imaging technologies, such as ^{1}H MRI, nuclear imaging, and FL imaging. ^{19}F MRI has been successfully employed in cell tracking [4–6], drug tracking [7,8], theranostic systems [9–12], etc., which significantly promotes biomedical research. Because ^{19}F MRI heavily relies on imaging agents as the signal source and functional entity, developing convenient, multifunctional, and highly sensitive ^{19}F MRI agents is of great importance for ^{19}F MRI and its application.

Since ^{19}F MRI was developed in 1977 [13], nanoemulsions of PFCs, such as perfluorooctyl bromide (PFOB), perfluorotributylamine (PFTBA), perfluorodecalin (PFD), etc., have been overwhelmingly employed as ^{19}F MRI agents [3,14,15]. Because of their high fluorine contents (usually over 60%), PFCs exhibit heavy fluorous properties [16,17] and thus suffer low emulsion stability, severe organ retention, difficulties in modification and formulation, extremely poor co-solubility of such functional agents as dyes, drugs, photosensitizers, etc. In ^{19}F MRI-monitored cell tracking and theranostic systems, the poor solubility of functional agents in heavy fluorous PFCs resulted in their tedious covalent conjugation to the emulsion components [18].

Thus, the co-solubilization of functional agents and ^{19}F signal compounds may significantly simplify the preparation of ^{19}F MRI agents. The co-solubility may also improve the performance of ^{19}F MRI agents

* Corresponding author.
** Corresponding author at: Hubei Province Engineering and Technology Research Center for Fluorinated Pharmaceuticals, School of Pharmaceutical Sciences, Wuhan University, Wuhan 430071, China.
E-mail addresses: zhengxing9166@sohu.com (X. Zheng), zxjiang@whu.edu.cn (Z.-X. Jiang).
[1] These authors contributed equally to this work

https://doi.org/10.1016/j.colsurfb.2022.112493
Received 24 December 2021; Received in revised form 23 March 2022; Accepted 5 April 2022
Available online 11 April 2022

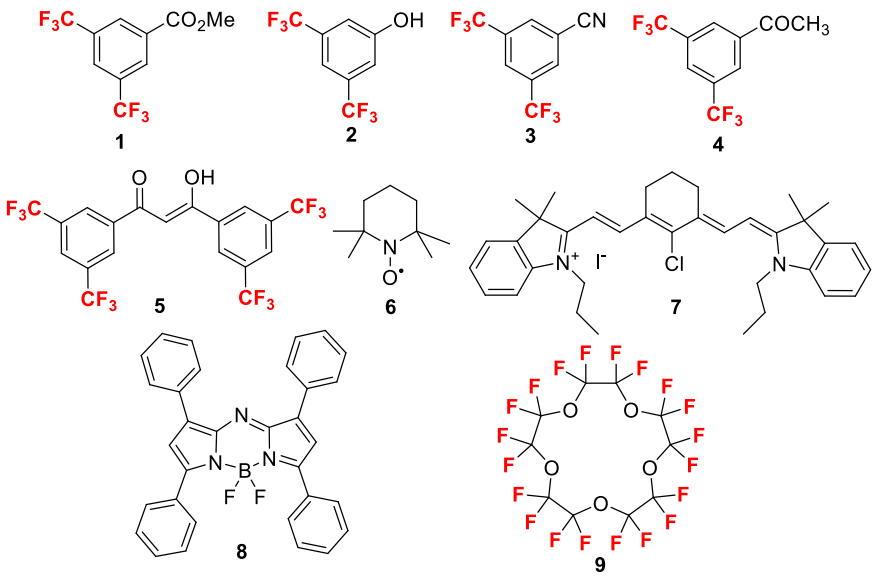

Fig. 1. Chemical structures of compounds **1–9**.

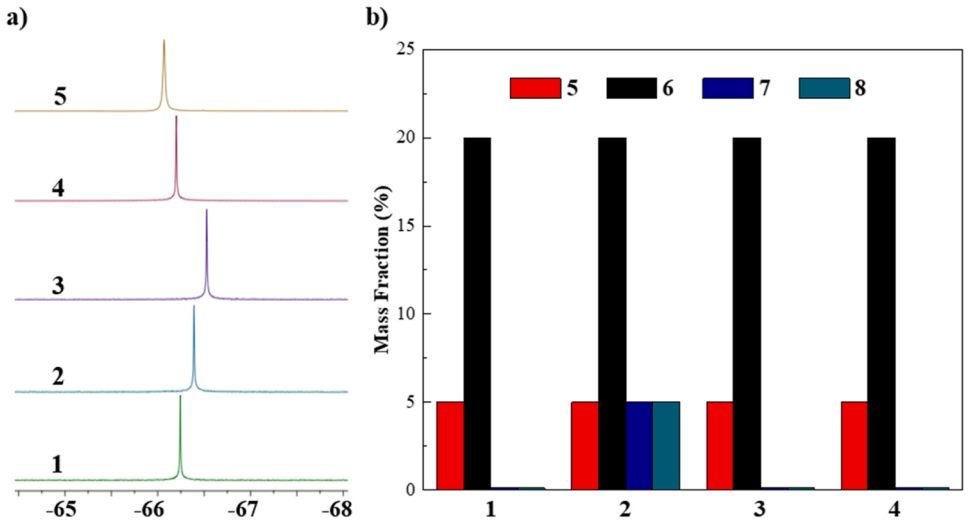

Fig. 2. Partial ^{19}F NMR spectra of reagents **1–4** and chelator **5** (a), and the co-solubility of agents **5–8** in reagents **1–4** (b).

by homogenizing the components to avoid the dyes' aggregate induced quenching (AIQ) of fluorescence and chelates' inhomogeneous paramagnetic relaxation enhancement (PRE) effect. Meanwhile, the much higher density of PFCs emulsions (usually 1.5–2.0 g/mL) than cell culture mediums leads to nanoemulsion droplet sedimentation, cell damage, and erroneous ^{19}F MRI results [19]. Moreover, even with high fluorine contents, the unsymmetrical arrangement of fluorines in most PFCs leads to their low ^{19}F MRI sensitivity and chemical shift-induced imaging artifacts [3]. Therefore, transforming heavy fluorous ^{19}F MRI signal molecules into normal organic molecules by reducing the fluorines, especially the non-signal-contribution fluorines[15], may address the issues mentioned above and maintain the ^{19}F MRI sensitivity.

Partially fluorinated compounds with multiple symmetrical fluorines may be good alternatives to PFCs in nanoemulsion-based ^{19}F MRI agents. Compared to PFCs, partially fluorinated compounds with much lower fluorine contents may have neglectable fluorous properties, lower density, high functional agent co-solubility, and ^{19}F MRI sensitivity. Among the partially fluorinated compounds, 3,5-bistrifluoromethylated phenyl derivatives are highly attractive. The strong and singlet ^{19}F signal from 6 symmetrical fluorines enables these compounds' high ^{19}F MRI sensitivity, while their relatively low fluorine contents (less than 50%) and the presence of polar functional groups, such as ester, ether, hydroxyl, and nitrile groups, may facilitate co-solubility of functional agents. Notably, the π-π interactions of their phenyl groups may slow down the molecular tumbling, shorten the relaxation times and thus improve the ^{19}F MRI sensitivity by reducing the data collection time. Further, convenient modification of the functional groups may incorporate novel functions, fine-tune relaxation times, and co-solubilities.

Tracking cells with ^{19}F MRI provides valuable real-time, selective, and quantitative cells information for cell biology and cell therapy [4–6]. The high ^{19}F MRI sensitivity of nanoemulsions is crucial for sensitive detection of cells and reducing perturbation on cells. At the same time, the FL imaging capability of nanoemulsions is usually required for in vitro cell study. Herein, we developed novel ^{19}F MRI-FL dual-imaging agents for cell tracking from readily available partially fluorinated compounds by tuning the co-solubility, relaxation times, and biocompatibility (Fig. 1). Partially fluorinated 3,5-bistrifluoromethylated phenyl derivatives **1–4**, commercially available liquid chemicals with low prices, were selected as ^{19}F MRI signal molecules and solvents for functional agents. Chelator **5** was designed as a paramagnetic ion

Table 1
Formulation ingredients, diameter, and PDI of nanoemulsions **E1–E13**.

Emulsions	Formulation ingredients[a]	Diameter (PDI)[b]
E1[c]	**1**, Lecithin, F68	412.6 (0.418)
E2	**1**, Lecithin, F68	215.9 (0.492)
E3[c]	**1**, E80, F68	86.4 (0.223)
E4[c]	**1**, S75, F68	108.9 (0.176)
E5[c]	**1**, Soybean oil, F68	172.4 (0.221)
E6[c]	**1**, Saffron oil, F68	162.4 (0.234)
E7[c]	**1**, Saffron oil, Lecithin	153.1 (0.337)
E8	**1**, S75, F68	92.1 (0.184)
E9	**1**, **5**, S75, F68	119.5 (0.188)
E10	**1**, **5**, **7**, S75, F68	126.0 (0.174)
E11	**1**, **5**, S75, F68, $FeCl_3$	120.5 (0.203)
E12	**1**, **5**, **7**, S75, F68, $FeCl_3$	112.1 (0.181)
E13	**1**, **5**, **7**, S75, F68, $FeCl_3$, RGD[d]	108.1 (0.219)

[a] Amount of ingredients in 4 mL water: 109 mg **1**, 1 mg **5**, 2 mg **7**, 80 mg S75 (or Lecithin), 40 mg F68.
[b] Size is the diameter in nm
[c] 40 mg of surfactant (S75, Lecithin, E80, Soybean oil, or Saffron oil) was used.
[d] RGD represented DSPE-PEG2000-RGDyC.

chelator to improve ^{19}F MRI sensitivity through the PRE effect, which contains the 3,5-bistrifluoromethylated phenyl groups to improve co-solubility and generate a united ^{19}F signal in chemicals **1–4**. Stable radical TEMPO **6** was used as potential dynamic nuclear polarization (DNP) agent for super sensitive hyperpolarized ^{19}F MRI [20,21]. FL dyes IR-780 **7** and aza-BODIPY **8** were employed to provide FL imaging capability for cell tracking. Perfluoro-15-crown-5 **9** was employed as a PFC control to show the difference between PFCs and partially fluorinated compounds.

2. Experimental section

The materials and specific experimental sections were in the Supplementary materials.

3. Results and discussions

With the ideas in mind, partially fluorinated reagents **1–4** and perfluoro-15-crown-5 **9** were obtained from commercial sources. Chelator **5** was conveniently synthesized from ester **1** and acetone **4** in just one step with a 45% yield on a multigram scale (Scheme S1).

As expected, all the fluorinated compounds **1–5** gave a sharp and singlet ^{19}F NMR peak around - 66 ppm from their multiple symmetrical fluorines (Fig. 2a). Then, the co-solubility of solid functional agents **5–8** in partially fluorinated reagents **1–4** were measured at the weight percentages of 1%, 5%, and 20%, respectively (Fig. 2b). In contrast, functional agents **5–8** showed neglectable solubility in perfluoro-15-crown-5 **9**. Chelator **5** showed solubility in reagents **1–4**, probably because they

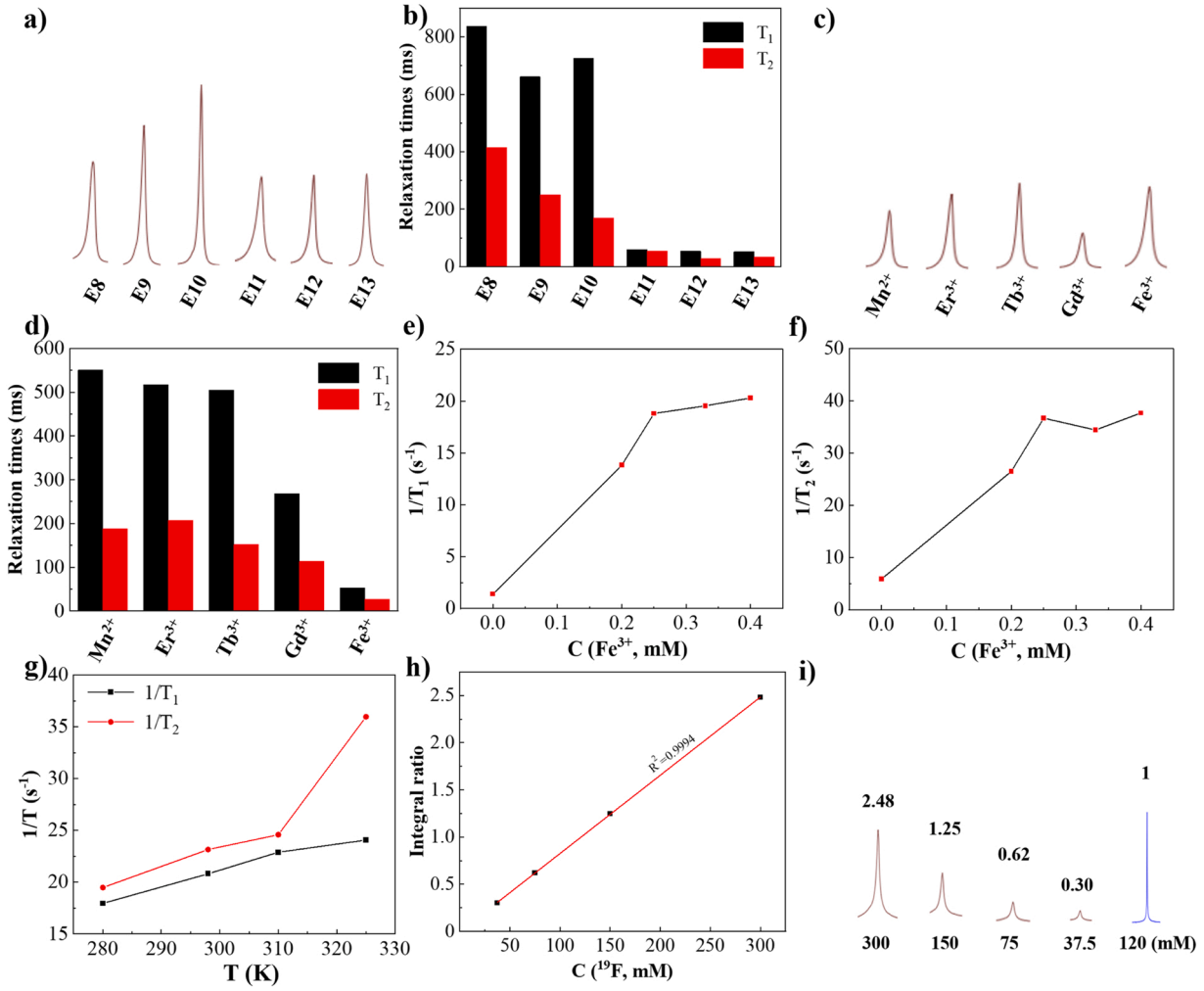

Fig. 3. Partial ^{19}F NMR spectra and ^{19}F relaxation times of nanoemulsions **E8** to **E13** (a, b) and **E10** with the indicated paramagnetic ions (c, d), Fe^{3+} to chelator **5** ratio-dependent T_1 (e) and T_2 (f) of **E12**, temperature-dependent T_1 and T_2 of **E11** (g), the plot of ^{19}F peak integral versus C(^{19}F) of **E10** using CF_3SO_3Na as internal standard (h) and partial ^{19}F NMR spectra of **E10** and CF_3SO_3Na solutions at the indicated concentrations (i).

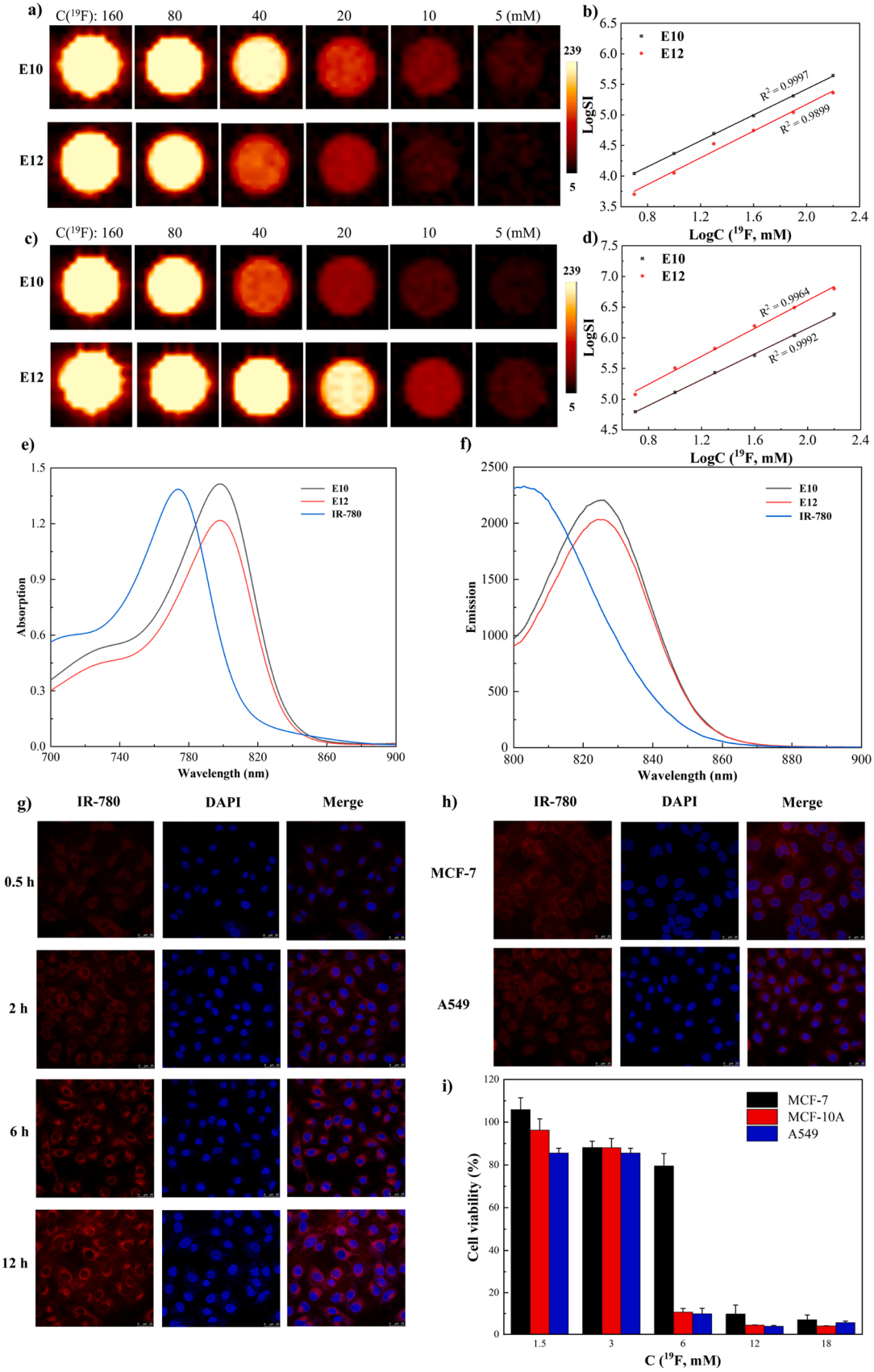

Fig. 4. ^{19}F density-weighted (a) and T_1-weighted (c) ^{19}F MRI phantom images and plot of LogSI versus LogC(^{19}F) (b, d) of **E10** and **E12**, UV absorption spectra (e) and FL emission spectra (f) of **7**, **E10** and **E12** at 5 μg/mL of **7**, confocal microscope images of A549 cells incubated with **E13** (g), A549 cells and MCF-7 cells after 2 h of incubation with **E12** (h), and cytotoxicity assay of **E12** in A549 cells, MCF-7 cells, and MCF-10A cells (i).

Table 2
Formulation ingredients, diameter, and PDI of nanoemulsions **E14**-**E20**.

Emulsions	Formulation ingredients[a]	Diameter (PDI)[b]
E14	**1**, Soybean oil, S75, F68	201.2 (0.199)
E15	**1**, **5**, Soybean oil, S75, F68	209.8 (0.173)
E16	**1**, **5**, Soybean oil, S75, F68, $FeCl_3$	238.0 (0.193)
E17	**1**, **5**, **8**, Soybean oil, S75, F68	222.8 (0.163)
E18	**1**, **5**, **8**, Soybean oil, S75, F68, $FeCl_3$	224.8 (0.125)
E19	**9**, **5**, **8**, Soybean oil, S75, F68	193.1(0.173)
E20	**9**, **5**, **8**, Soybean oil, S75, F68, $FeCl_3$	203.3 (0.237)

[a] Amount of ingredients in 4 mL water: 109 mg **1** or **9**, 1 mg **5**, 1 mg **8**, 200 mg soybean oil, 40 mg S75, 40 mg F68.
[b] Size is the diameter in nm.

share the same 3,5-bis(trifluoromethyl)phenyl structures. TEMPO **6** was well dissolved in reagents **1–4** with at least 20% weight percentages. Unfortunately, IR-780 **7** and aza-BODIPY **8** exhibited poor solubility in reagents **1–4** due to their charge, high polarity and aggregation tendency. The considerable solubility of chelator **5** in reagents **1–4** may facilitate the homogeneous distribution of paramagnetic ions to efficiently shorten relaxation times and improve ^{19}F MRI sensitivity.

Among reagents **2–4**, phenol **2** gives an unpleasant smell while nitrile **3** and ketone **4** carry biologically reactive functional groups, which may lead to toxicity. Esters widely exist in biological systems and ester **1** can be easily modified into other esters and amides, which was selected for the downstream study. Ester **1**, chelator **5**, and IR-780 **7** were employed to formulate nanoemulsions for potential ^{19}F MRI-FL dual-imaging cell tracking. After an initial screening of the surfactants for ester **1**, S75 and F68 were found to provide monodisperse and homogeneous nanoemulsion **E8** with a diameter of 92 nm and a polydispersity index (PDI) of 0.184 (Table 1). The incorporation of chelator **5** and IR-780 **7** enlarged the particle size to about 120 nm, but the monodispersity of nanoemulsion was well maintained. After adding ferric chloride to nanoemulsions **E9** and **E10**, the visible color changes indicated the capture of iron (III) (Fe^{3+}) by chelator **5**, from which monodisperse paramagnetic nanoemulsions **E11** and **E12** were prepared.

Dynamic light scattering (DLS) and transmission electron microscopy (TEM) showed the monodispersity and spherical shape of nanoemulsions **E10** and **E12**, respectively (Fig. S2a and S2b).

As expected, nanoemulsions **E8** to **E13** gave a strong and singlet ^{19}F NMR peak around - 65.2 ppm, respectively (Fig. 3a). ^{19}F relaxation times of the nanoemulsions were then measured (Fig. 3b). As expected, aromatic ester **1** had much shorter relaxation times (**E8**: $T_1 = 838$ ms, $T_2 = 415$ ms) in nanoemulsion than those of PFCs (nanocapsule of PFOB: $T_1 = 1305$ ms, $T_2 = 695$ ms) under similar conditions [22]. The addition of chelator **5** dramatically shortened the T_1 by 21%, further demonstrating the π-π interactions as efficient relaxation times shorten strategy. Among the selected paramagnetic ions, including Mn^{2+}, Er^{3+}, Tb^{3+}, Gd^{3+} and Fe^{3+}, Fe^{3+} showed the highest efficacy in reducing the relaxation times (Fig. 3c and 3d). Incorporating Fe^{3+} at a 1: 4 ratio to chelator **5** overwhelmingly reduced the T_1 by up to 93% (Fig. 3e and 3f). The short T_1 (53 ms) and T_2 (27 ms) of nanoemulsion **E12** would significantly promote its ^{19}F MRI sensitivity by reducing the data collection time. A temperature-dependent relaxation times reduction was observed on **E11** when elevating the temperature from 280 K to 325 K, indicating improved temperature may improve the ^{19}F MRI sensitivity (Fig. 3g). Finally, quantification of the fluorines in nanoemulsion **E10** with ^{19}F NMR was investigated. Using sodium trifluoromethanesulfonate (CF_3SO_3Na) as an internal standard, the ^{19}F peak integrals of **E10** were proportional to the ^{19}F concentrations (Fig. 3h and 3i) and, therefore, the fluorine concentration of nanoemulsions may be accurately quantified by ^{19}F NMR signal intensity.

Next, the ^{19}F MRI and FL imaging capabilities of nanoemulsions **E10** and **E12** were investigated. The ^{19}F density-weighted ^{19}F MRI phantom images showed that **E10** and **E12** are highly ^{19}F MRI sensitive and detectable at low ^{19}F concentrations of 5 mM and 10 mM with a data collection time of 256 s, respectively (Fig. 4a). Notably, **E10** showed a slightly higher ^{19}F MRI sensitivity than **E12**, which may be related to the

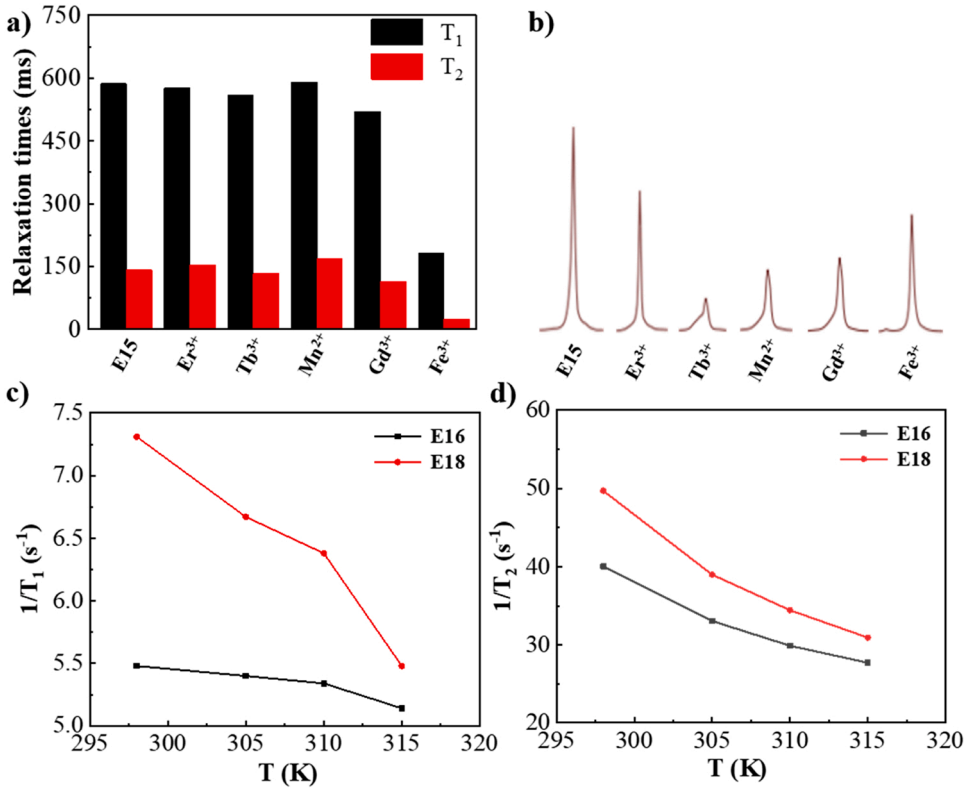

Fig. 5. Effects of paramagnetic ions on the relaxation times (a) and ^{19}F NMR spectra (b) of **E15**, temperature-dependent T_1 (c) and T_2 (d) of **E16** and **E18**.

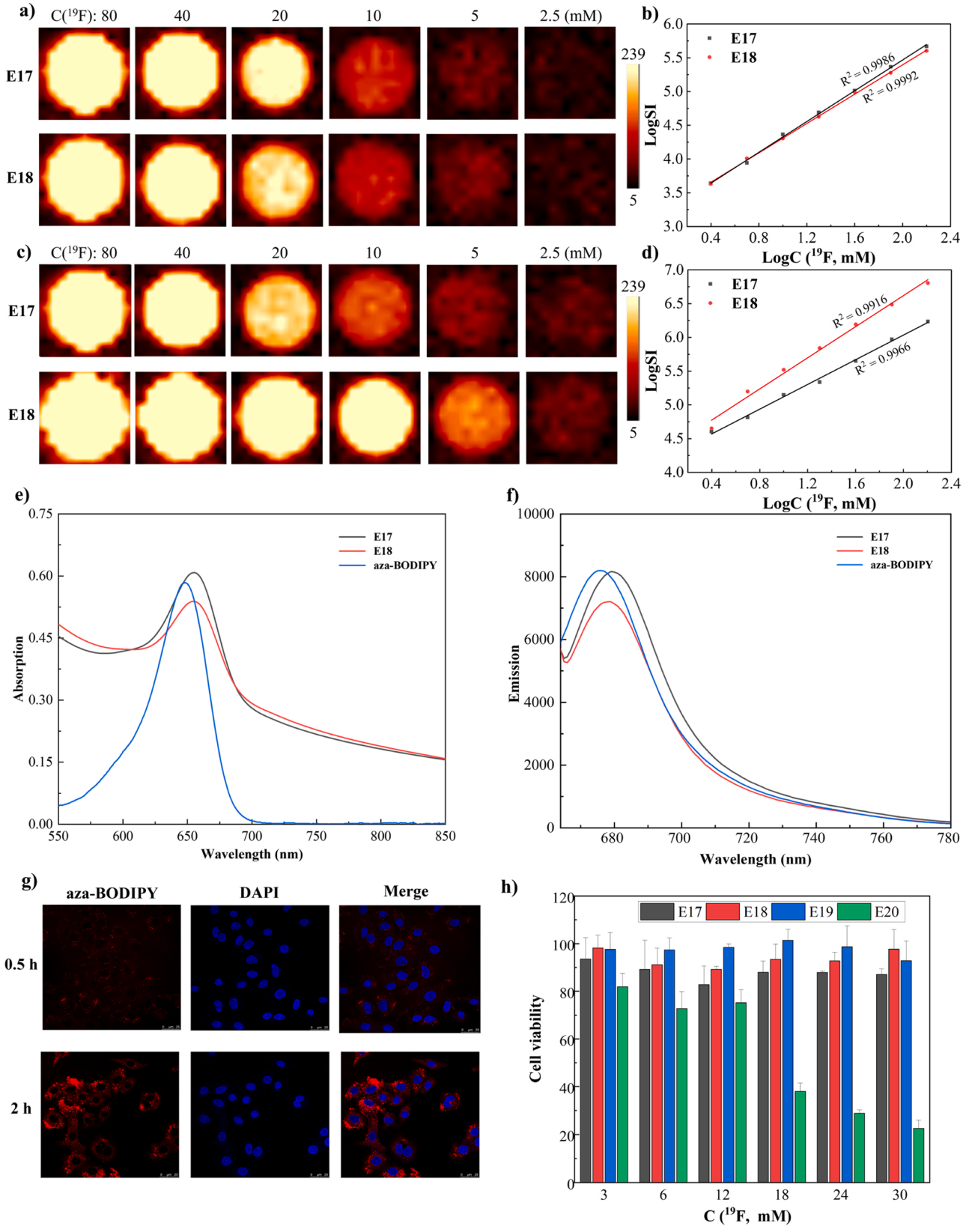

Fig. 6. ^{19}F density-weighted ^{19}F MRI (a), T_1-weighted ^{19}F MRI phantom images (c), the plot of LogSI versus LogC(^{19}F) (b, d) of **E17** and **E18**, and UV absorption spectra (e) and FL emission spectra (f) of **8**, **E17** and **E18** at an **8** concentration of 2.5 μg/mL, confocal microscope images of A549 cells incubated with **E18** (g), and cytotoxicity assay of **E17–E20** in A549 cells (h).

Fe^{3+}-induced nanoemulsion structural perturbations in **E12**. In contrast, **E12** has a much higher ^{19}F MRI sensitivity than **E10** in the T_1-weighted ^{19}F MRI with a detectable ^{19}F concentration of 5 mM, which clearly showed the ^{19}F MRI sensitivity enhancement by the PRE-effect of Fe^{3+} (Fig. 4c). In both cases, the logarithm of ^{19}F MRI signal intensity (LogSI) was indeed proportional to the logarithm of ^{19}F concentration (LogC (^{19}F), Fig. 4b and 4d), which enables the accurate quantification of the fluorines in nanoemulsions with ^{19}F MRI. Compared to IR-780 **7**, significant red-shifts of about 24 nm were observed from the UV absorption spectra of nanoemulsions **E10** and **E12** (Fig. 4e), which facilitate the exiting of the nanoemulsion in the near-infrared region. Meanwhile, maximum FL emission peaks around 824 nm with significant red-shifts of 20 nm compared to IR-780 were also observed in the FL spectra of **E10** and **E12** (Fig. 4f). The high UV absorption and FL emission intensity of **E10** and **E12** indicated the homogeneous distribution of IR-780 in the nanoemulsion without aggregation.

With the high ^{19}F MRI sensitivity and FL capability, the nanoemulsions were employed in cell studies. Confocal microscope images indicated the efficient uptake of nanoemulsion **E13**, which was surface modified with cancer cell-targeting peptide DSPE-PEG_{2000}-RGDyC, by human lung cancer A549 cells after 12 h of incubation (Fig. 4g). Even without the targeting peptide, **E12** showed efficient uptaken by both human breast cancer MCF-7 cells and A549 cells after 2 h of incubation (Fig. 4h). With the aid of nucleus dye DAPI, **E12** and **E13** were found in the cytoplasm after being uptaken by the cells. Then, the cytotoxicity of **E12** was evaluated in A549 cells, MCF-7 cells, and normal human breast MCF-10A cells. Unfortunately, **E12** exhibited high cytotoxicity toward A549 cells and MCF-10A cells above the ^{19}F concentration of 6 mM (Fig. 4i). After a series of control experiments, it was found that the relatively low stability of **E12** in the cell culture medium may lead to cytotoxicity.

To avoid unexpected cytotoxicity, we redesigned the formulation of nanoemulsions. Soybean oil was employed to improve the stability, and IR-780 **7** was replaced with less phototoxic aza-BODIPY **8** (Table 2) [23]. The addition of soybean oil yielded much larger nanoemulsions (around 200 nm) than previous ones, while the presence of aza-BODIPY had little impact on the particle size and PDI. After a 14-day stability study with DLS, nanoemulsions **E17** were found to be stable in water and cell culture medium containing fetal bovine serum (Fig. S2). Consistent with previous results, Fe^{3+} was the most effective paramagnetic ion in reducing relaxation times (Fig. 5a and 5b). Compared to its IR-780 counterpart, nanoemulsion **E18** with aza-BODIPY had longer T_1 and shorter T_2, which suggested possible interactions between aza-BODIPY and Fe^{3+}. Interestingly, the temperature-dependent relaxation times measurement showed longer relaxation times at higher temperatures (Fig. 5c and 5d), suggesting the impact of soybean oil-based formulation on relaxation times, especially at elevated temperatures.

With an appropriate particle size of 225 nm and a low PDI of 0.125, nanoemulsion **E18** with short relaxation times (T_1 = 137 ms, T_2 = 20 ms) was selected for the imaging study. Further, competitive chelating agent EDTA was added to nanoemulsion **E18** with 24 h of stirring, which led to the increased of relaxation times (T_1 = 363 ms, T_2 = 110 ms), indicating a reversed diffusion of Fe^{3+} from the nanoemulsion particles to the EDTA solution [6]. ^{19}F density-weighted ^{19}F MRI phantom images showed comparable ^{19}F MRI sensitivity for **E17** and paramagnetic **E18** (Fig. 6a), which were detected at a ^{19}F concentration of 2.5 mM with a data collection time of 160 s. With the PRE-effect to short data collection times, paramagnetic **E18** showed a much higher ^{19}F MRI sensitivity than **E17** in the T_1-weighted ^{19}F MRI phantom images (Fig. 6c). In both cases, LogSI was proportional to LogC (^{19}F) (Fig. 6b and 6d), ideal for downstream quantitative ^{19}F MRI. In contrast, neglectable relaxation time differences were detected in perfluoro-15-crown-5 nanoemulsion **E19** and **E20** after the addition of $FeCl_3$ (Fig. S3), which suggested the perfluoro-15-crown-5 was not able to dissolve chelator **5**. Compared to aza-BODIPY, the UV absorption and FL emission were well maintained in **E17** and **E18** (Fig. 6e and 6f).

Finally, the cell uptake of nanoemulsion **E18** and cytotoxicity of nanoemulsion **E17–E20** were evaluated on A549 cells. Confocal microscope images indicated that **E18** can be uptaken by A549 cells after 2 h of incubation (Fig. 6g). Fortunately, **E17–E18** showed high biocompatibility at a fluorine concentration of up to 30 mM after 12 h of incubation **E17–E18** in A549 cells (Fig. 6h), suggesting that soybean oil and aza-BODIPY may significantly reduce cytotoxicity. Therefore, **E18** would be a potential agent for ^{19}F MRI-FL dual-imaging cell tracking. In comparison, **E20** showed high toxicity in A549 cells because Fe^{3+} was not well dissolved in the nanoparticles (Fig. 6h), which further indicated the low solubility of chelator **5** in perfluoro-15-crown-5.

4. Conclusion

In this study, we have developed novel ^{19}F MRI-fluorescence dual-imaging nanoemulsions with high ^{19}F MRI sensitivity, stability, and biocompatibility for cell tracking from partially fluorinated reagents. Without any chemical modification, the commercially available reagent, methyl 3,5-bis(trifluoromethyl)benzoate, was directly used in ^{19}F MRI for the first time, in which the six symmetrical fluorines enable high ^{19}F MRI sensitivity while significantly reducing the fluorine content for co-solubility of functional agents, low nanoemulsion density and high nanoemulsion stability. In the partially fluorinated nanoemulsions, π-π interactions and chelated paramagnetic Fe^{3+} induce ultra-short T_1 for highly sensitive and quantitative ^{19}F MRI, while the incorporated fluorescence imaging facilitates convenient in vitro cell studies. The biocompatibility of nanoemulsion was conveniently tuned by the highly adjustable formulation, e.g., the addition of soybean oil and switch of FL dyes. Although many nanoemulsions have been developed for ^{19}F MRI cell tracking in the last two decades, the problematic PFCs and complicated synthetic molecules in these systems hamper ^{19}F MRI cell tracking development and application. This study provides an alternative strategy for the convenient construction of highly sensitive ^{19}F MRI cell tracking agents.

CRediT authorship contribution statement

Kexin Chen: Synthesis, Formulation, Characterization, and Cell study. **Tingjuan Wu:** Formulation and cell study. **Mou Jiang:** $^{1}H/^{13}C/^{19}F$ NMR and ^{19}F MRI. **Anfeng Li:** Cell culture. **Xingxing Peng:** Cell culture. **Shizhen Chen:** Project administration. **Zhigang Yang:** Project supervision. **Xin Zhou:** Project design and funding acquisition. **Xing Zheng:** Writing-original draft. **Zhong-Xing Jiang:** Project design, Writing-review & editing.

Declaration of Competing Interest

The authors declare that they have no known competing financial interests or personal relationships that could have appeared to influence the work reported in this paper.

Acknowledgments

We are thankful for financial support from the National Natural Science Foundation of China (22077098 and 91859206), the National Key R&D Program of China (2018YFA0704000), Natural Science Foundation of Hunan (2021JJ80015), Hunan Provincial Hengyang Joint Fund (2020JJ6052), Laboratory of Tea and Health of Hengyang (202150083704).

Appendix A. Supporting information

Supplementary data associated with this article can be found in the online version at doi:10.1016/j.colsurfb.2022.112493.

References

[1] J. Ruiz-Cabello, B.P. Barnett, P.A. Bottomley, J.W.M. Bulte, Fluorine (^{19}F) MRS and MRI in biomedicine, NMR Biomed. 24 (2) (2011) 114–129.

[2] I. Tirotta, V. Dichiarante, C. Pigliacelli, G. Cavallo, G. Terraneo, F.B. Bombelli, P. Metrangolo, G. Resnati, ^{19}F magnetic resonance imaging (MRI): From design of materials to clinical applications, Chem. Rev. 115 (2) (2015) 1106–1129.

[3] L. Wu, F. Liu, S. Liu, X. Xu, Z. Liu, X. Sun, Perfluorocarbons-based ^{19}F magnetic resonance imaging in biomedicine, Int. J. Nanomed. 15 (2020) 7377–7395.

[4] M. Srinivas, A. Heerschap, E.T. Ahrens, C.G. Figdor, I.J.M. de Vries, ^{19}F MRI for quantitative in vivo cell tracking, Trends Biotechnol. 28 (7) (2010) 363–370.

[5] M. Srinivas, P. Boehm-Sturm, C.G. Figdor, I.J. de Vries, M. Hoehn, Labeling cells for in vivo tracking using ^{19}F MRI, Biomaterials 33 (34) (2012) 8830–8840.

[6] Q. Peng, Y. Li, S. Bo, Y. Yuan, Z. Yang, S. Chen, X. Zhou, Z.-X. Jiang, Paramagnetic nanoemulsions with unified signals for sensitive ^{19}F MRI cell tracking, Chem. Commun. 54 (47) (2018) 6000–6003.

[7] Y.B. Yu, Z.-X. Jiang, Prospect of ^{19}F MRI-guided drug delivery, J. Pharm. Drug Deliv. Res. 1 (2012) 1.

[8] S. Bo, Y. Yuan, Y. Chen, Z. Yang, S. Chen, X. Zhou, Z.-X. Jiang, In vivo drug tracking with ^{19}F MRI at therapeutic dose, Chem. Commun. 54 (31) (2018) 3875–3878.

[9] S.K. Patel, Y. Zhang, J.A. Pollock, J.M. Janjic, Cyclooxgenase-2 inhibiting perfluoropoly (ethylene glycol) ether theranostic nanoemulsions-in vitro study, PLoS One 8 (2) (2013), e55802.

[10] S.H. Shin, E.J. Park, C. Min, S.I. Choi, S. Jeon, Y.H. Kim, D. Kim, Tracking perfluorocarbon nanoemulsion delivery by ^{19}F MRI for precise high intensity focused ultrasound tumor ablation, Theranostics 7 (3) (2017) 562–572.

[11] Y. Zhang, S. Bo, T. Feng, X. Qin, Y. Wan, S. Jiang, C. Li, J. Lin, T. Wang, X. Zhou, Z.-X. Jiang, P. Huang, A versatile theranostic nanoemulsion for architecture-dependent multimodal imaging and dually augmented photodynamic therapy, Adv. Mater. 31 (21) (2019), 1806444.

[12] H. Zhang, Q. Yu, Y. Li, Z. Yang, X. Zhou, S. Chen, Z.-X. Jiang, Fluorinated cryptophane-A and porphyrin-based theranostics for multimodal imaging-guided photodynamic therapy, Chem. Commun. 56 (25) (2020) 3617–3620.

[13] G.N. Holland, P.A. Bottomley, W.S. Hinshaw, ^{19}F magnetic resonance imaging, J. Magn. Reson. 28 (1) (1977) 133–136.

[14] J.C. Knight, P.G. Edwards, S.J. Paisey, Fluorinated contrast agents for magnetic resonance imaging: a review of recent developments, RSC Adv. 1 (2011) 1415–1425.

[15] T. Wu, A. Li, K. Chen, X. Peng, J. Zhang, M. Jiang, S. Chen, X. Zheng, X. Zhou, Z.-X. Jiang, Perfluoro-tert-butanol: a cornerstone for high-performance fluorine-19 magnetic resonance imaging, Chem. Commun. 57 (63) (2021) 7743–7757.

[16] J.A. Gladysz, D.P. Curran, Fluorous chemistry: from biphasic catalysis to a parallel chemical universe and beyond, Tetrahedron 58 (20) (2002) 3823–3825.

[17] M. Cametti, B. Crousse, P. Metrangolo, R. Milani, G. Resnati, The fluorous effect in biomolecular applications, Chem. Soc. Rev. 41 (2012) 31–42.

[18] J.M. Janjic, M. Srinivas, D.K.K. Kadayakkara, E.T. Ahrens, Self-delivering nanoemulsions for dual fluorine-19 MRI and fluorescence detection, J. Am. Chem. Soc. 130 (9) (2008) 2832–2841.

[19] S.K. Patel, J. Williams, J.M. Janjic, Cell labeling for ^{19}F MRI: new and improved approach to perfluorocarbon nanoemulsion design, Biosensors 3 (3) (2013) 341–359.

[20] M.E. Halse, P.T. Callaghan, A dynamic nuclear polarization strategy for multi-dimensional Earth's field NMR spectroscopy, J. Magn. Reson. 195 (2) (2008) 162–168.

[21] A. Dey, A. Banerjee, Unusual Overhauser dynamic nuclear polarization behavior of fluorinated alcohols at room temperature, J. Phys. Chem. B 123 (49) (2019) 10463–10469.

[22] C. Giraudeau, J. Flament, B. Marty, F. Boumezbeur, S. Mériaux, C. Robic, M. Port, N. Tsapis, E. Fattal, E. Giacomini, F. Lethimonnier, D.L. Bihan, J. Valette, A new paradigm for high-sensitivity ^{19}F magnetic resonance imaging of perfluorooctylbromide, Magn. Reson. Med. 63 (2010) 1119–1124.

[23] D. Chen, Z. Zhong, Q. Ma, J. Shao, W. Huang, X. Dong, Aza-BODIPY-based nanomedicines in cancer phototheranostics, ACS Appl. Mater. Interfaces 12 (24) (2020) 26914–26925.